RSC Advances

ROYAL SOCIETY OF CHEMISTRY

www.rsc.org/advances

Journal Name

ARTICLE

Synthesis of Core-Shell Structured Ag_3PO_4@Benzoxazine Soft Gel Nanocomposites and their Photocatalytic Performance

Received 00th January 20xx,
Accepted 00th January 20xx

DOI: 10.1039/x0xx00000x

www.rsc.org/

Yue Hu, Shaping Huang, Xinsheng Zheng*, Feifei Cao*, Ting Yu, Geng Zhang, Zhidong Xiao, Jiangong Liang, Yichi Zhang

In photocatalysis investigation, it remains a significant challenge to improve the interface properties and enhance the stability of photocatalysts. To address this challenge, we have prepared the core-shell structured Ag_3PO_4@benzoxazine soft gel nanocomposites, in which Ag_3PO_4 nanoparticles are coated with uniform benzoxazine monomers via a facile solution self-assembly method. The benzoxazine monomers are attached to the surface of Ag_3PO_4 nanoparticles by coordination interaction between the amino group of the benzoxazine monomers and Ag^+ ions on the surface of Ag_3PO_4, and the soft gel shell is formed via the interaction of hydrogen bonds between the benzoxazine monomers. The nanocomposites exhibit higher visible-light photocatalytic stability than the bare Ag_3PO_4 nanoparticles under the same reaction conditions. Both experimental evidences and electrochemical calculations reveal that the high photocatalytic stability of Ag_3PO_4@benzoxazine soft gel nanocomposites mainly originates from the silver amine complex ion formed in the interface between the core and the shell. The integration of photocatalysts with the advantages of soft gels can provide a new way to improve the interface properties of Ag_3PO_4 catalyst and facilitate to realize the long-standing goal of performing chemical synthesis using the sunlight.

Introduction

On earth, a lot of chemical reactions can be driven by sunlight and carried out in hydrogels, such as reactions occurring in plants. Scientists have aspired to synthesize molecules in the same manner that plants do.[1,2] Natural photosynthesis converts solar energy to chemical energy by means of two large pigment-protein complexes: photosystem I (PSI) and photosystem II (PSII).[3] The active sites of PSII are Mn_4Ca-cluster and a number of amino acid residues.[4] The amino acid residues can provide ligands to the metal ions and act to facilitate hydrogen bonding networks which almost certainly play a key role in the deprotonation of the substrate water molecules.[5,6] So we put up Ag_3PO_4 nanoparticles (Ag_3PO_4 NPs) instead of Mn_4Ca-cluster and benzoxazine soft gels with a certain amount of amino groups to mimic natural photosynthesis. Only molecular mimics can facilitate direct measurement and then photocatalysis mechanism can be explored.

To date, numerous semiconductor photocatalysts have been studied in water splitting and oxidative decomposition of various organic pollutants.[7,8] TiO_2 is one of the most renowned photocatalyst because of its chemical stability, nontoxicity and photocatalytic activity.[9,10] However, TiO_2 only responds to high-energy UV light, which limits its practical applications.[11] So TiO_2–based composite photocatalysts have been widely studied through doping with foreign elements to modify the photonic band gap,[12-14] adding metal free phthalocyanines and various dyes for light sensitization,[15,16] and combining with other semiconductors (such as ZnO, CeO_2, etc.)[17-20] to enhance the photogenerated charges separation. Meanwhile, some novel materials, such as ZnO, Cu_2O, graphitic carbon nitride (g-C_3N_4), Bi- and Ag-based photocatalysts have been studied and demonstrate excellent photoelectrochemical activities.[21-25] Among them, Ag_3PO_4 is a visible-light-absorbing semiconductor and can achieve quantum efficiencies of up to 90% at wavelengths greater than 420 nm.[26] Unfortunately, Ag_3PO_4 NPs are slightly soluble in aqueous solution and tend to undergo photocorrosion in the photocatalytic reaction, which decrease the visible-light photocatalytic activity and stability.[27] To address these issues, Ag_3PO_4 NPs are dispersed on metal oxide, bentonite, reduced graphite oxide sheets, hydroxyapatite, C_3N_4 sheets, polyaniline, and so on.[28-34] However, Ag_3PO_4 NPs attached on the support surfaces have high surface energy and tend to aggregate into larger particles, leading to the loss of catalytic activity during photocatalytic reactions.[35] A good synthetic design may significantly improve the catalytic performance of Ag_3PO_4 semiconductor, such as Ag_3PO_4@AgX (X=Cl, Br, I) core-shell heterostructures which effectively protect the Ag_3PO_4 from corrosion and maximize the Ag_3PO_4-support interaction through the three-dimensional contact between the Ag_3PO_4 core and the AgX shell.[36] As known, polymer gels utilized as structured reaction vessels and reusable photocatalysts have drawn much attention over recent years.[37,38]

[a] Department of Chemistry, College of Science, Huazhong Agricultural University, Wuhan 430070, P. R. China. E-mail:xszheng@mail.hzau.edu.cn; caofeifei@mail.hzau.edu.cn

† Footnotes relating to the title and/or authors should appear here.
Electronic Supplementary Information (ESI) available: [details of any supplementary information available should be included here]. See DOI: 10.1039/x0xx00000x

David et al. developed organophotocatalysis in nanostructured soft gel materials as tunable reaction vessels.[39] Mishra and co-workers fabricated a photocatalyst based on Eu^{3+}-doped ZnS-SiO_2 and sodium alginate core-shell nanocomposites.[40] Zhu et al. reported a TCNQ@TiO_2 core-shell photocatalyst to decompose phenol.[41] Here, we choose the benzoxazine monomers as a coating material owing to its special structural and polymer gel properties. The structure of benzoxazine monomers is an oxazine ring attached to a benzene ring, and benzoxazine monomers further form physical gels by the intermolecular bond.[42] The benzoxazine soft gels possess immense molecular design flexibility for its high active surface area and excellent diffusion properties.[43,44] The fast molecular mass transport in the soft gel shells could facilitate molecules to access the active sites located within nanocomposites and reduce the residence time of molecules in catalysts, leading to enhanced reaction rates and slower deactivation.[45,46] So the benzoxazine soft gel shell could dramatically improve the interface properties of Ag_3PO_4 core.

In this paper, for the first time, we demonstrate that Ag_3PO_4 NPs are coated with benzoxazine monomers to form Ag_3PO_4@benzoxazine soft gel (Ag_3PO_4@BSG) core-shell nanocomposites by molecular self-assembly in solution. Interestingly, the Ag_3PO_4@BSG nanocomposites possess higher visible-light photocatalytic stability than bare Ag_3PO_4. The integration of the photocatalysts with the advantages of soft gels could provide a new tool to create multifunctional materials for photocatalysis.[47-50]

Results and discussion

Characterization of nanocomposites

The formation process of the core-shell Ag_3PO_4@BSG nanocomposites is illustrated in Scheme 1. Through the molecular self-assembly, in which the Ag_3PO_4 NPs dispersed in toluene medium, reacting with the benzoxazine monomers (Fig. S1 ESI†) dissolved in the methanol solution, the Ag_3PO_4@BSG nanocomposites are obtained. By changing the starting material molar ratio of benzoxazine monomers/Ag_3PO_4 from 10% to 40%, a series of Ag_3PO_4@BSG nanocomposites are obtained, and referred to as Ag_3PO_4@BSG-X (10, 20, 30, and 40). Next, take the Ag_3PO_4@BSG-30 nanocomposites as an example, their morphology and structure are investigated by transmission electron microscopy (TEM), X-ray diffraction (XRD) and Raman spectrum. The TEM images show that the products exhibit sphere-like shape (Fig. 1A). Additionally, some nanocomposites are entangled with each other. It can be clearly seen from Fig. 1B that the as-prepared Ag_3PO_4@BSG-30 nanocomposites possess a typical core-shell structure, in which an Ag_3PO_4 NP core of about 80-120 nm in diameter is coated with a uniform benzoxazine soft gel shell of about 15-25 nm in thickness. Fig. 1C shows the XRD patterns of the as-prepared bare Ag_3PO_4 and Ag_3PO_4@BSG-X nanocomposites. Curve (a) is the XRD pattern of the prepared bare Ag_3PO_4, in which all the intense diffraction peaks correspond to the typical body-centered cubic structure of Ag_3PO_4 (JCPDS No.06-0505). Curve (b)-(e) are the XRD pattern of Ag_3PO_4@BSG-X nanocomposites. Compared with curve (a), there are no differences in the locations for the diffraction peaks of Ag_3PO_4, demonstrating that the introduction of benzoxazine monomers does not affect the crystal structure of Ag_3PO_4 in the nanocomposites. In the Raman spectra (Fig. 1D), the bare Ag_3PO_4 shows an intense sharp band at 910 cm^{-1} ascribed to the PO_4^{3-} symmetric stretching vibrations.[51] Meanwhile, the peaks located at ~529 and 617 cm^{-1} correspond to the benzoxazine ring breathing, while the characteristic peak at 813 cm^{-1} is attributed to C–N–C symmetric stretch vibrations of benzoxazine monomers.[52] Additionally, the band near 1000 cm^{-1} is assigned to C–C stretching vibration of benzoxazine ring, and the bands at 1262 and 1368 cm^{-1} are attributed to C–O–C or C–N–C asymmetric stretch vibrations of benzoxazine ring.[52] The bands at 1451 and 1596 cm^{-1} are assigned to C–C stretching vibration of benzene ring. In the Raman spectrum of the Ag_3PO_4@BSG nanocomposites, there are the PO_4^{3-} vibration and some characteristic peaks of the benzoxazine ring structures, suggesting that the existence of benzoxazine in the Ag_3PO_4@BSG nanocomposites. More importantly the characteristic peak of C–N–C symmetric stretch vibrations disappears, suggesting the existence of coordination interaction between Ag^+ ions on the surface of Ag_3PO_4 and amino groups of the benzoxazine monomers to form silver amine complex compound.

To further investigate the interaction between Ag_3PO_4 and benzoxazine in the nanocomposites, X-ray photoelectron spectroscopy (XPS) of the Ag_3PO_4@BSG-30 nanocomposites was performed (Fig. 2). The peaks of Ag $3d_{5/2}$ and Ag $3d_{3/2}$ are located at 373.7 and 367.7 eV.[53] These two bands could be further deconvoluted into two peaks respectively. The strong peaks at 373.9 and 367.8 eV are assigned to Ag^+ of Ag_3PO_4, while there are two new weak peaks at 372.6 and 366.5 eV. It is well-known that the binding energy of its inner shell electrons reduces when the atom obtain electrons. It can be inferred that Ag^+ of Ag_3PO_4 obtains electrons from amine groups of benzoxazine monomers in the composites to form silver amine complex compound. This XPS result is in good agreement with the above Raman spectra result.

The formation of Ag_3PO_4@BSG nanocomposites is heavily influenced by the dispersing media and the starting molar ratio of benzoxazine monomers/Ag_3PO_4. When the benzoxazine monomers in methanol solution are added into the suspension of Ag_3PO_4 in toluene dispersing medium, benzoxazine monomers are directionally arranged and attached to the surface of Ag_3PO_4 NPs due to the coordination interaction between the amino groups of the benzoxazine monomers and Ag^+ ions on the surface of Ag_3PO_4 as well as the hydrophobic interaction between the non polar groups of benzoxazine monomers and dispersing medium toluene. As the result, the polar portion of benzoxazine monomers is toward the surface of Ag_3PO_4 while its non polar portion is toward the dispersing medium toluene. As the evaporation of methanol that is the excellent solvent for the benzoxazine monomers in the synthesis system, the benzoxazine monomers attached to the surface of Ag_3PO_4 NPs have formed a physical soft gel shell via the interaction of hydrogen bonds between the benzoxazine monomers. There are some characteristic peaks of benzoxazine ring in the Raman spectrum of the Ag_3PO_4@BSG-30 nanocomposites, demonstrating that the oxazine rings in benzoxazine monomers are fully retained and the ring-opening polymerization of benzoxazine monomers does

not take place. Because the temperature of ring-opening polymerization of benzoxazine monomers is about 230 °C,[54] whereas the temperature for preparation of Ag_3PO_4@BSG nanocomposites is only 80 °C.

To support this proposed mechanism, a series of control experiments were carried out including the selection of dispersing media and changing the molar ratios of the benzoxazine monomers/Ag_3PO_4. The property of dispersing media is found to be a critical factor in generating core-shell Ag_3PO_4@BSG nanostructures. Using water as dispersing medium instead of toluene, no distinct benzoxazine soft gel shell on the surface of Ag_3PO_4 NPs was observed although the benzoxazine monomers can attach to the surface of Ag_3PO_4, likely due to the polarity of water hindering the directional arrangement of benzoxazine monomers on the surface of Ag_3PO_4 NPs. While methyl-silicone oil was used as dispersing medium under the same conditions, the benzoxazine monomers aggregated easily and the core-shell Ag_3PO_4@BSG nanocomposites cannot be obtained because the benzoxazine monomers was insoluble in methyl-silicone oil. The polarity of toluene is between water and methyl-silicone oil, and the benzoxazine monomers is partially soluble in toluene. This causes favorable directional arrangement of the benzoxazine monomer in the dispersing media. By varying the starting molar ratio of benzoxazine monomers to Ag_3PO_4 NPs ranging from 10% to 40%, the shell thicknesses of benzoxazine soft gel were tuned from about 10 to 95 nm as shown in Fig. 3. When this molar ratio is below 10%, there is only partial BSG shell found. The properties of the core-shell Ag_3PO_4@BSG nanocomposites, such as photocatalytic stability, are even considerably influenced by the molar ratio of benzoxazine monomers/Ag_3PO_4. Furthermore, the thickness control of BSG-shell could be used for molecular diffusion studies in the future.

Photocatalytic performance

The photocatalytic properties of the core-shell Ag_3PO_4@BSG nanocomposites were evaluated using the degradation of rhodamine B (RhB) under visible light irradiation as model reactions. In addition, the commercial C_3N_4 widely accepted as popular visible light photocatalyst was used as the sample for comparisons. As shown in Fig. 4, no RhB is decomposed without a photocatalyst, indicating the stable property of RhB under visible light irradiation. Using benzoxazine monomer as a catalyst, no obvious photocatalytic activity is found, indicating benzoxazine monomers has no effect on photocatalytic degradation of RhB. From Fig. 4c and d, both Ag_3PO_4 and Ag_3PO_4@BSG-30 nanocomposites are able to adsorb RhB, which are beneficial to the photodecomposition of RhB. The photocatalytic activity of the Ag_3PO_4@BSG-30 nanocomposites is much better than the commercial C_3N_4 and slightly lower than the bare Ag_3PO_4. It can be concluded that the photocatalytic activity of the core-shell Ag_3PO_4@BSG-30 nanocomposites comes from Ag_3PO_4 and the benzoxazine soft gel shell coating on the Ag_3PO_4 NPs scarcely affects the photocatalytic activity of the nanocomposites.

To further evaluate their stability and reusability, the bare Ag_3PO_4 and the core-shell Ag_3PO_4@BSG-30 nanocomposites were recycled and reused for five recycles. As shown in Fig. 5, the photocatalytic RhB degradation performance of the bare Ag_3PO_4 continues to decrease with the increase of the recycles. The bare Ag_3PO_4 can degrade 100% RhB in 20 min at the first recycle, but only degrade 50% of RhB in 80 min at the fifth recycle. However, the photocatalytic degradation performance of the core-shell Ag_3PO_4@BSG-30 nanocomposites does not exhibit significant changes with the increasing recycles. In the first recycle, the nanocomposites can degrade 100% RhB in 60 min and still 100% RhB in 80 min at the fifth recycle. To identify the generality of this result, the photocatalytic stability of the core-shell Ag_3PO_4@BSG-30 nanocomposites is further investigated for photocatalytic methyl orange (MO) degradation experiment (Fig. S2 ESI†). The results are completely similar to the RhB degradation experiments. It reveals that the introduction of benzoxazine soft gel shell can significantly enhance the photocatalytic degradation stability of Ag_3PO_4 NPs.

The effects of starting material molar ratios of the benzoxazine monomers/Ag_3PO_4 on the photocatalytic activity and stability of the nanocomposites are investigated. The photocatalytic activities of the Ag_3PO_4@BSG-X (10, 20, 30, 40) nanocomposites are nearly the same (Fig. S3 ESI†), and they can completely degrade RhB in 30 min. The amounts of benzoxazine monomers have slightly influence on the photocatalytic activity, but great influence on the photocatalytic stability. As shown in Fig. 6, the photocatalytic stability of the nanocomposites is constantly improved as increasing the material molar ratio of benzoxazine monomers to Ag_3PO_4 from 10% to 30%, whereas the photocatalytic stabilities of the Ag_3PO_4@BSG-40 nanocomposites are slightly less than that of the Ag_3PO_4@BSG-30 nanocomposites in the fourth and fifth recycle. For the core-shell Ag_3PO_4@BSG-10 and Ag_3PO_4@BSG-20, the photocatalytic stability continues to decrease with increasing photocatalytic recycles. These results suggest that when the molar ratio of benzoxazine monomers/Ag_3PO_4 is less than 30%, the formed soft gel shell that contains too few benzoxazine monomers is not enough to prevent Ag_3PO_4 core from photo-corrosion and dissolution during the photocatalytic reaction. But excessive benzoxazine monomers might trigger reactants and products stranded in the photocatalysts such as the Ag_3PO_4@BSG-40 nanocomposites, leading to the depression of photocatalytic stability.

Photocatalytic mechanism

XRD spectra and TEM images of Ag_3PO_4 and Ag_3PO_4@BSG nanocomposites after repeating photocatalytic degradation of RhB were also recorded to understand the photocatalytic mechanism of Ag_3PO_4@BSG nanocomposites. Fig. 7A shows that there are very few diffraction peaks of metallic Ag observed from the Ag_3PO_4@BSG nanocomposites reused in three successive recycles (Fig. 7A, b) compared with the fresh nanocomposites (Fig. 7A, a). After used in five successive experiments, some diffraction peaks of metallic Ag are observed from the Ag_3PO_4@BSG nanocomposites (Fig. 7A, c). The TEM images of re-used Ag_3PO_4@BSG nanocomposites show that the benzoxazine soft gel shells of the nanocomposites are nearly unchanged after three cyclic experiments (Fig. 7C) and become slightly loose after five successive recycles (Fig. 7D) compared with the fresh photocatalyst (Fig. 7B). These results demonstrate a relatively high stability of the soft gel shells. To further confirm the stability of the soft gel shells, the Raman

spectras of Ag_3PO_4@BSG nanocomposites before and after photocatalytic reaction were investigated (Fig. S4 ESI†). No evident changes could be observed in the the characteristic peaks of benzoxazine monomers, indicating that the benzoxazine monomers is very stable on the surface of the nanocomposites. This result is consistent with the above TEM results.

Bi and coworkers previously reported that pure Ag_3PO_4 crystals were completely destroyed and decomposed into small and irregular fragments when they were used as photocatalysts for the degradation of MO.[36] After pure Ag_3PO_4 NPs were reused in three successive methyl blue degradation experiments, the calculated weight fraction of metallic Ag (W_A) derived from the reduction of Ag_3PO_4 is 81.4%.[51] For comparison, the core-shell Ag_3PO_4@BSG nanocomposites exhibit both the photocatalytic stability and the structural stability during the degradation of RhB and MO. The results come from two reasons. First, benzoxazine soft gel coated on the surface of Ag_3PO_4 can inhibit the dissolution of Ag_3PO_4 in aqueous solution, which will enhance its structural stability. Second, the silver amine complex compound formed by the Ag^+ ions on the surface of Ag_3PO_4 and amino groups of the benzoxazine monomers may inhibit photocorrosion of Ag_3PO_4 into metallic Ag during the photocatalytic process. However, the photocatalytic activity of Ag_3PO_4@BSG nanocomposites is slightly lower than the bare Ag_3PO_4. We know that the photocatalytic activity is closely related to solar absorption, charge separation and catalytic conversion. Therefore, the benzoxazine soft gel coated on the surface of Ag_3PO_4 may inhibit solar adsorption and could be unfavourable for the photocatalytic activity of the as-synthesized composite materials.

To investigate the photocatalytic mechanism of the Ag_3PO_4@BSG nanocomposites in detail, reactive species trapping experiments were also performed by the degradation of RhB. In this study, three different chemicals, p-benzoquinone (BO, a $\cdot O_2^-$ radical scavenger), triethanolamine (AO, a hole scavenger) and tert-butanol (TBA, a ·OH radical scavenger) are employed respectively. As shown in Fig. 8, the addition of TBA does not affect the decolorization rate of RhB over Ag_3PO_4@BSG-30 nanocomposites, suggesting that ·OH is not main reactive species in the photocatalytic process. On the contrary, the photocatalytic degradation of RhB is obviously suppressed after the addition of AO and BO, suggesting that h^+ and $\cdot O_2^-$ are the primary active species.

According to the Nernst equation in electrochemistry, the potential of silver amine complex ion/metallic silver can be calculated by

$$\varphi = \varphi^{\theta}_{Ag^+/Ag} - \frac{RT}{F}\ln(K_{SC}\cdot a^2_{amine})$$

where $\varphi^{\theta}_{Ag^+/Ag}$ is the standard potential of silver ion/metallic silver (0.80 V) versus the NHE, R is the gas constant (8.314 J K^{-1} mol^{-1}), T is the reaction temperature (298 K), F is the Faraday constant (96485 C), K_{SC} is the stability constant of silver amine complex (1.7×10^7 at 298K),[55] a_{amine} is the activity (approximating the concentration) of amino groups on the interface between Ag_3PO_4 nanoparticle core and benzoxazine soft gel shell and is set to about 0.1 mol dm^{-3}, which about 1000 times the concentration of silver ions on the interface according to estimation of Ag_3PO_4 solubility product constant (1.4×10^{16}). Based on the calculation via the above equation, the potential of silver amine complex ion/metallic silver is about 0.49 V versus the NHE, whereas the conduction band potential of Ag_3PO_4 is 0.45 V versus the NHE.[56] This means that the potential of silver amine complex ion/silver attached on the surface of Ag_3PO_4 nanoparticle is more positive than the potential of Ag_3PO_4 conduction band. Based on the above results, a possible mechanism for photocatalytic degradation of RhB on Ag_3PO_4@BSG-30 nanocomposites is illustrated in Fig. 9. The photo-generated electrons in the Ag_3PO_4 conduction band under visible light irradiation should easily transfer to the silver amine complex ion, and then the electrons reduce O_2 molecule absorbed on the surface of the silver amine complex ion. Furthermore, the photo-generated holes in the Ag_3PO_4 valence band are able to oxidize organic dye directly because of its strong oxidation. The transfer of the photo-generated electrons in this way effectively protects Ag_3PO_4 to avoid their photoreduction ($Ag^+ + e^- \rightarrow Ag$), leading to an improvement of photocatalytic stability of the core-shell Ag_3PO_4@BSG photocatalyst. In this manner, the photoexcited electron-holes in the nanocomposites are separated efficiently, thereby leading to the excellent photocatalytic activity and stability.

In addition, the fabrication of Ag_3PO_4-based composites are generally the combination of Ag_3PO_4 with an effective electronic conductor such as graphene,[57] graphene oxide,[58] polyaniline,[34] and so forth, to improve photocatalytic activity and stability of Ag_3PO_4. Interestingly, benzoxazine monomers instead of an electronic conductor are attached to Ag_3PO_4 NPs to construct the core-shell Ag_3PO_4@BSG nanocomposites with high visible-light photocatalytic stability. This can greatly broaden the range of materials for synthesis of Ag_3PO_4-based composites and more importantly provide a new way to improve the interface properties of Ag_3PO_4 catalyst. There is no doubt that improving the interface properties of photocatalysts facilitates the realization the long-standing goal of performing chemical synthesis using the sunlight.

Conclusions

In summary, the core-shell structured Ag_3PO_4@BSG nanocomposites can be readily fabricated by a facile solution self-assembly method. Interestingly, the Ag_3PO_4@BSG nanocomposites are a novel type of effective photocatalysts for the degradation of RhB and MO under visible light irradiation, and their photocatalytic stability is far higher than the bare Ag_3PO_4 NPs. The formation of the silver amine complex ion between Ag_3PO_4 and benzoxazine monomers efficiently increases the separation of electron-hole pairs, thus avoiding the photoreduction of Ag_3PO_4. Furthermore, h^+ and $\cdot O_2^-$ play the major role in photocatalysis process. To the best of our knowledge, the core-shell structured Ag_3PO_4@BSG nanocomposites are the first example that the soft gels are attached onto the surface of visible light photocatalyst. The nature of the soft gel shell in Ag_3PO_4@BSG nanocomposites might have great influence on the outcome of a photocatalytic reaction, and further detailed study of the photocatalytic mechanism of the soft gel catalyst is needed in the following works.

Acknowledgements

We are grateful for the financial support of the National Natural Science Foundation of China (51173059, 21303064) and Wuhan Chenguang Science and Technology Project for Young Experts (2015070404010192).

Experimental section

Sample preparation

Synthesis of the Ag_3PO_4 NPs. In a typical synthesis, $AgNO_3$ aqueous solution (5 mL, 0.035 mol/L) was added dropwise to $Na_2HPO_4 \cdot 12H_2O$ aqueous solution (75 mL, 0.035 mol/L) under stirring. The obtained yellow precipitates were separated by centrifuge, followed by washing with deionized water for several times.

Synthesis of the benzoxazine monomer. Firstly, 1 mol equiv of melamine, 2 mol equiv of phenol, and 6 mol equiv of formaldehyde were added into solvent mixture consisted of water and methanol (volume ratio of 1:1) under magnetic stirring in a round-bottom flask at 85 °C for 6 h. The solvents were removed from the reaction mixture by decompressing distillation at 55 °C. Finally, a low-viscosity, transparent colorless liquid was obtained (Fig. S1, ESI†).

Synthesis of the core-shell structured Ag_3PO_4@BSG nanocomposites. Typically, Ag_3PO_4 NPs (418.0 mg, 1 mmol) were dispersed into 70 mL toluene medium to form a suspension. Benzoxazine monomer (107.0 mg, 0.3 mmol) dissolved in 50 mL methanol was added slowly into the suspension at 65 °C for 3 h under vigorous stirring. Then the products were centrifuged and dried at 80 °C for 12 h to obtain the core-shell structured Ag_3PO_4@benzoxazine soft gel nanocomposites designated as Ag_3PO_4@BSG-30 (the starting material molar ratio of benzoxazine monomers/Ag_3PO_4 is 30%). Follow the same routine, Ag_3PO_4@BSG-10, Ag_3PO_4@BSG-20, and Ag_3PO_4@BSG-40 (the molar ratios of benzoxazine monomers/Ag_3PO_4 are 10%, 20% and 40%) nanocomposites were synthesized, respectively.

Characterization

The morphologies of the as-synthesized Ag_3PO_4@BSG nanocomposites were examined by TEM (Hitachi H-7650) with an accelerating voltage of 100 kV. The phases of the obtained samples were investigated using XRD (Bruker D8 Advance X-ray diffractometer) with Cu Ka radiation. The acceleration voltage and the applied current were 40 kV and 40 mA, respectively. Raman spectra were recorded at room temperature using a micro-Raman spectrometer (Renishaw Invia) in the backscattering geometry with a 532 nm laser as an excitation source. XPS measurements were recorded with a Multilab-2000 electron spectrometer and the spectra were calibrated to the C 1s peak at 284.8 eV as a reference.

Photocatalytic degradation of RhB and MO

For photocatalytic degradation of RhB, 50 mg photocatalyst was dispersed in 100 mL of rhodamine B (RhB) solution (4 mg/L). The suspension was then stirred vigorously in the dark for 30 min to establish an adsorption-desorption equilibrium. A 300 W Xe lamp was employed as simulated sunlight source with a cutoff filter (λ>400 nm). About 4 mL of the suspension was taken out at given time intervals and separated through centrifugation (10000 rpm, 10 min). The concentration of RhB aqueous was determined with a Shimadzu UV-2450 spectrophotometer by measuring the absorbance at 553 nm. The stability and reusability of bare Ag_3PO_4 NPs and Ag_3PO_4@BSG-30 nanocomposites were tested by repeating photocatalytic degradation of RhB and MO. The degradation of MO (4 mg/L) was carried out under the same way except that the amount of catalyst is 100 mg. After one recycle, the photocatalyst was filtrated and washed thoroughly with deionized water, and then fresh RhB or MO solution was added to begin the next recycle.

Active species trapping experiments

For the trapping of photogenerated active species during photocatalytic process, hydroxyl radicals (·OH), superoxide radical ($\cdot O_2^-$) and holes (h^+) were investigated using tertiary butanol (TBA, 1mM), p-benzoquinone (BO, 1mM) and triethanolamine (AO, 1mM) respectively. The process of active species trapping experiment was similar to the RhB photodegradation experiment. Scavengers were introduced into the RhB solution respectively before adding the photocatalyst.

References

1 L. Sun, *Science*, 2015, **348**, 635-636.
2 J. C. Colmenares and R. Luque, *Chem. Soc. Rev.*, 2014, **43**, 765-778.
3 P. Jordan, P. Fromme, H. T. Witt, O. Klukas, W. Saenger and N. Krausz, *Nature*, 2001, **411**, 909-917.
4 A. Zouni, H. T. Witt, J. Kern, P. Fromme, N. Krauss, W. Saenger and P. Orth, *Nature*, 2001, **409**, 739-743.
5 J. Barber, *Chem. Soc. Rev.*, 2009, **38**, 185-196.
6 K. N. Ferreira, T. M. Iverson, K. Maghlaoui, J. Barber and S. Iwata, *Science*, 2004, **303**, 1831-1838.
7 J. Hong, X. Xia, Y. Wang and R. Xu, *J. Mater. Chem.*, 2012, **22**, 15006-15012.
8 A. Di Paola, E. Garcia-Lopez, G. Marci and L. Palmisano, *J. hazard. mater.*, 2012, **211-212**, 3-29.
9 A. Fujishima, *nature*, 1972, **238**, 37-38.
10 A. Fujishima, X. Zhang and D. A. Tryk, *Surf. Sci. Rep.*, 2008, **63**, 515-582.
11 K. L. Schulte, P. A. DeSario and K. A. Gray, *Appl. Catal., B*, 2010, **97**, 354-360.
12 J. C. Yu, J. Yu, W. Ho, Z. Jiang and L. Zhang, *Chem. Mater.*, 2002, **14**, 3808-3816.
13 T. Ihara, M. Miyoshi, Y. Iriyama, O. Matsumoto and S. Sugihara, *Appl. Catal., B*, 2003, **42**, 403-409.
14 C. Burda, Y. Lou, X. Chen, A. C. S. Samia, J. Stout and J. L. Gole, *Nano Lett.*, 2003, **3**, 1049-1051.
15 J. He, G. Benkö, F. Korodi, T. Polívka, R. Lomoth, B. Åkermark, L. Sun, A. Hagfeldt and V. Sundström, *J. Am. Chem. Soc.*, 2002, **124**, 4922-4932.

16 W. M. Campbell, A. K. Burrell, D. L. Officer and K. W. Jolley, *Coord. Chem. Rev.*, 2004, **248**, 1363-1379.
17 J. Matos, E. García-López, L. Palmisano, A. García and G. Marcì, *Appl. Catal., B*, 2010, **99**, 170-180.
18 B. M. Reddy, A. Khan, Y. Yamada, T. Kobayashi, S. Loridant and J. C. Volta, *J. Phys. Chem. B*, 2003, **107**, 5162-5167.
19 H. Zhang, X. Lv, Y. Li, Y. Wang and J. Li, *ACS Nano* , 2009, **4**, 380-386.
20 W. Wang, P. Serp, P. Kalck and J. L. Faria, *Appl. Catal., B,* 2005, **56**, 305-312.
21 B. Li and Y. Wang, *J. Phys. Chem. C*, 2009, **114**, 890-896.
22 J. Y. Ho and M. H. Huang, *J. Phys. Chem. C*, 2009, **113**, 14159-14164.
23 F. Dong, L. Wu, Y. Sun, M. Fu, Z. Wu and S. Lee, *J. Mater. Chem.*, 2011, **21**, 15171-15174.
24 M. Shang, W. Wang, S. Sun, L. Zhou and L. Zhang, *J. Phys. Chem. C*, 2008, **112**, 10407-10411.
25 J. Tang, W. Gong, T. Cai, T. Xie, C. Deng, Z. Peng and Q. Deng, *RSC Adv.*, 2013, **3**, 2543-2547.
26 Z. Jiao, Y. Zhang, H. Yu, G. Lu, J. Ye and Y. Bi, *Chem. Commun.*, 2013, **49**, 636-638.
27 S. Kumar, T. Surendar, A. Baruah and V. Shanker, *J. Mater.Chem. A*, 2013, **1**, 5333-5340.
28 Z. M. Yang, G. F. Huang, W. Q. Huang, J. M. Wei, X. G. Yan, Y. Y. Liu, C. Jiao, Z. Wan and A. Pan, *J. Mater. Chem. A*, 2014, **2**, 1750-1756.
29 Y. Song, Y. Lei, H. Xu, C. Wang, J. Yan, H. Zhao, Y. Xu, J. Xia, S. Yin and H. Li, *Dalton trans.*, 2015, **44**, 3057-3066.
30 J. Ma, J. Zou, L. Li, C. Yao, T. Zhang and D. Li, *Appl. Catal., B*, 2013, **134-135**, 1-6.
31 P. Dong, Y. Wang, B. Cao, S. Xin, L. Guo, J. Zhang and F. Li, *Appl. Catal., B*, 2013, **132-133**, 45-53.
32 X. Hong, X. Wu, Q. Zhang, M. Xiao, G. Yang, M. Qiu and G. Han, *Appl. Surf. Sci.*, 2012, **258**, 4801-4805.
33 S. Kumar, T. Surendar, A. Baruah and V. Shanker, *J. Mater. Chem. A*, 2013, **1**, 5333-5340.
34 Y. Bu and Z. Chen, *ACS Appl. Mater. Interfaces*, 2014, **6**, 17589-17598.
35 C. Tang, E. Liu, J. Fan, X. Hu, Y. Ma and J. Wan, *RSC Adv.*, 2015, **5**, 91979-91987.
36 Y. Bi, S. Ouyang, J. Cao and J. Ye, *Phys. Chem. Chem. Phys.*, 2011, **13**, 10071-10075.
37 S. Bag, P. N. Trikalitis, P. J. Chupas, G. S. Armatas and M. G. Kanatzidis, *Science*, 2007, **317**, 490-493.
38 J. Y. Sun, X. Zhao, W. R. Illeperuma, O. Chaudhuri, K. H. Oh, D. J. Mooney, J. J. Vlassak and Z. Suo, *Nature*, 2012, **489**, 133-136.
39 J. Bachl, A. Hohenleutner, B. B. Dhar, C. Cativiela, U. Maitra, B. Konig and D. D. Diaz, *J. Mater. Chem. A*, 2013, **1**, 4577-4588.
40 E. S. Agorku, H. Mittal, B. B. Mamba, A. C. Pandey and A. K. Mishra, *Int. J. Biol. Macromol.*, 2014, **70**, 143-149.
41 W. Jiang, M. Zhang, J. Wang, Y. Liu and Y. Zhu, *Appl. Catal., B*, 2014, **160**, 44-50.
42 P. Calvert, *Adv. Mater.*, 2009, **21**, 743-756.
43 González-Rodríguez, J. R. Suárez, J. A. Varela and C. Saá, *Angew. Chem., Int. Ed.*, 2015, **54**, 2724-2728.
44 S. Wang, W. C. Li, G. P. Hao, Y. Hao, Q. Sun, X. Q. Zhang and A. H. Lu, *J. Am. Chem. Soc.*, 2011, **133**, 15304-15307.
45 F. Svec and J. M. J. Fréchet, *Science*, 1996, **273**, 205-211.
46 C. Y. Hui, Y. Y. Lin, F. C. Chuang, K. R. Shull and W. C. Lin, *J. Polym. Sci., Part B: Polym. Phys.*, 2006, **44**, 359-370.
47 H. Kang, A. C. Trondoli, G. Zhu, Y. Chen, Y. J. Chang, H. Liu, Y. F. Huang, X. Zhang and W. Tan, *ACS Nano*, 2011, **5**, 5094-5099.
48 U. T. D. Thuy, N. Q. Liem, C. M. A. Parlett, G. M. Lalev and K. Wilson, *Catal. Commun.*, 2014, **44**, 62-67.
49 M. Marguet, C. Bonduelle, S. Lecommandoux, *Chem. Soc. Rev.*, 2013, **42**, 512-529.
50 C. Zhang, C. Chen, H. Dong, J. R. Shen, H. Dau and J. Zhao, *Science*, 2015, **348**, 690-693.
51 P. Dong, Y. Wang, B. Cao, S. Xin, L. Guo, J. Zhang and F. Li, *Appl. Catal., B*, 2013, **132-133**, 45-53.
52 I. Hamerton, K. Ennis, B. J. Howlin and L. T. McNamara, *React. Funct. Polym.*, 2013, **73**, 1612-1624.
53 Y. Liu, L. Fang, H. Lu, Y. Li, C. Hu and H. Yu, *Appl. Catal., B*, 2012, **115–116**, 245-252.
54 J. Shi, X. Zheng, L. Xie, F. Cao, Y. Wu and W. Liu, *Eur. Polym. J.*, 2013, **49**, 4054-4061.
55 David R Lide. CRC Handbook of chemistry and physics. CRC Press: America.
56 Z. Chen, W. Wang, Z. Zhang and X. Fang, *J. Phys. Chem. C*, 2013, **117**, 19346-19352.
57 X. Yang, H. Cui, Y. Li, J. Qin, R. Zhang and H. Tang, *ACS Catal.*, 2013, **3**, 363-369.
58 Q. Liang, Y. Shi, W. Ma, Z. Li and X. Yang, *Phys. Chem. Chem. Phys.*, 2012, **14**, 15657-15665.

Figures

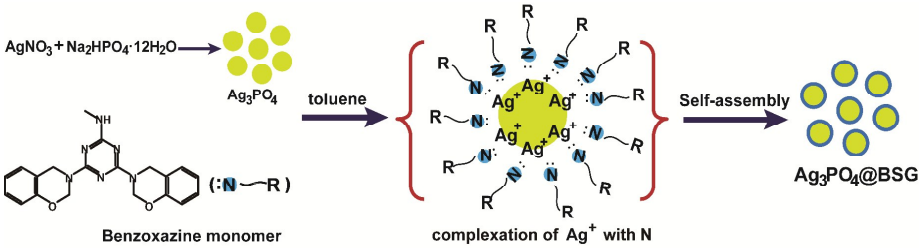

Scheme 1. Synthetic procedure for the Ag_3PO_4/BSG nanocomposites.

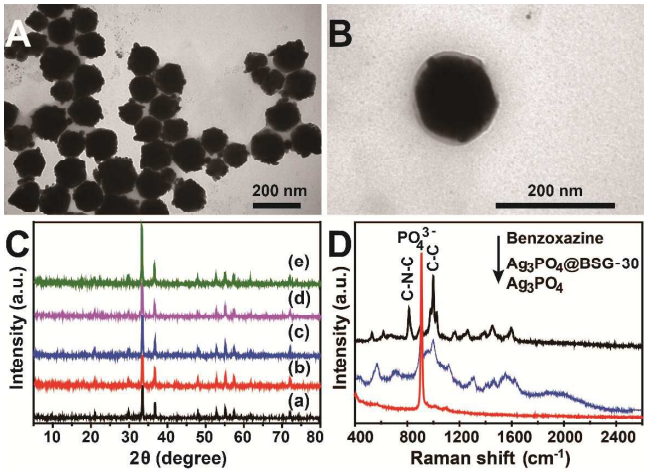

Fig. 1 (A, B) TEM images of the Ag_3PO_4@BSG-30 nanocomposites. (C) XRD patterns of Ag_3PO_4, Ag_3PO_4@BSG-10, Ag_3PO_4@BSG-20, Ag_3PO_4@BSG-30 and Ag_3PO_4@BSG-40 nanocomposites (curve (a)─(e)). (D) Raman spectra of benzoxazine monomers, Ag_3PO_4, and the Ag_3PO_4@BSG-30 nanocomposites.

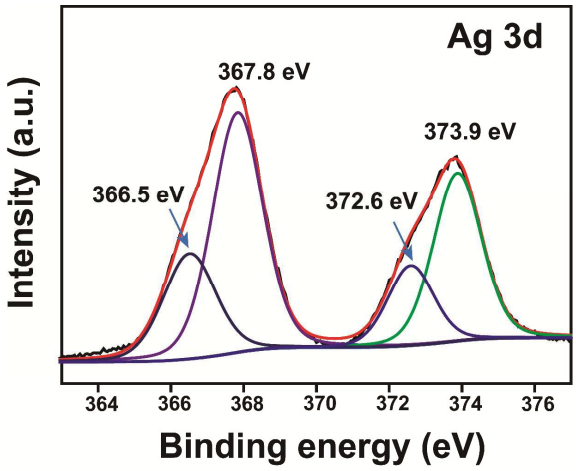

Fig. 2 High-resolution Ag 3d XPS spectra of the fresh Ag_3PO_4@BSG-30 nanocomposites.

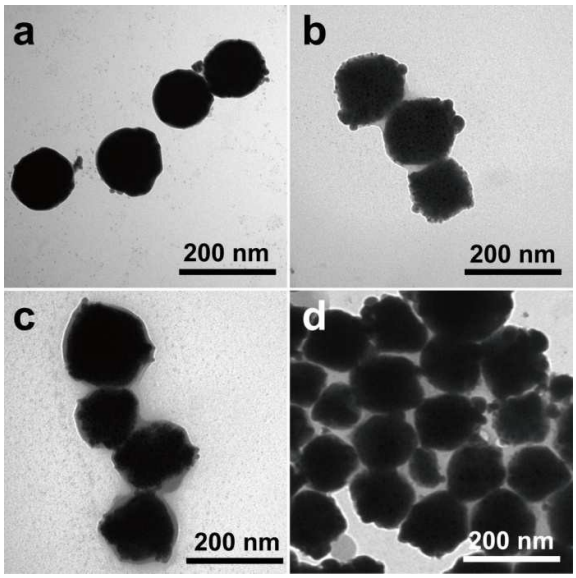

Fig. 3 TEM images of (a) Ag_3PO_4@BSG-10, (b) Ag_3PO_4@BSG-20, (c) Ag_3PO_4@BSG-30, and (d) Ag_3PO_4@BSG-40 nanocomposites.

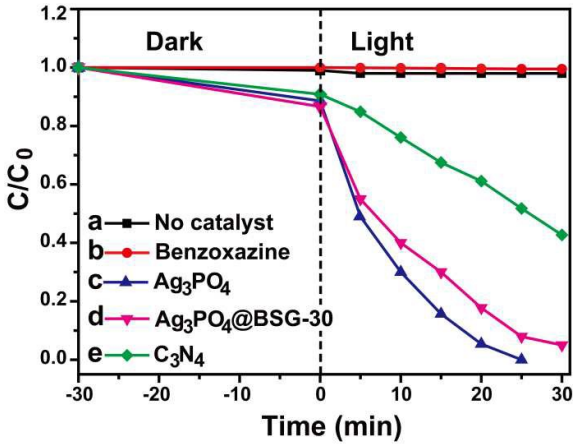

Fig. 4 Photocatalytic RhB degradation efficiency of (a) no catalyst, (b) benzoxazine monomers, (c) Ag_3PO_4, (d) Ag_3PO_4@BSG-30 nanocomposites, and (e) C_3N_4 under visible light irradiation.

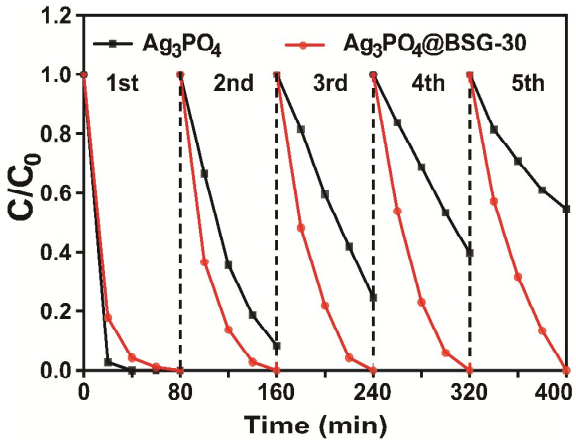

Fig. 5 Photocatalytic stabilities of the bare Ag_3PO_4 and the Ag_3PO_4@BSG-30 nanocomposites as photocatalysts for the degradation of RhB (4mg/L) under visible light irradiation.

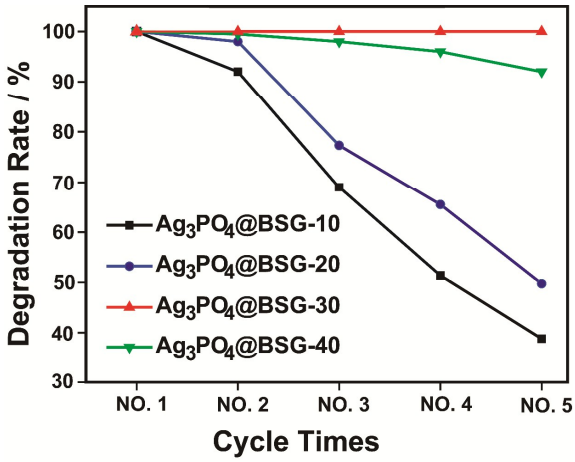

Fig. 6 Cycling performance of the Ag_3PO_4@BSG-10, Ag_3PO_4@BSG-20, Ag_3PO_4@BSG-30, and Ag_3PO_4@BSG-40 nanocomposites for the degradation of RhB under visible light irradiation.

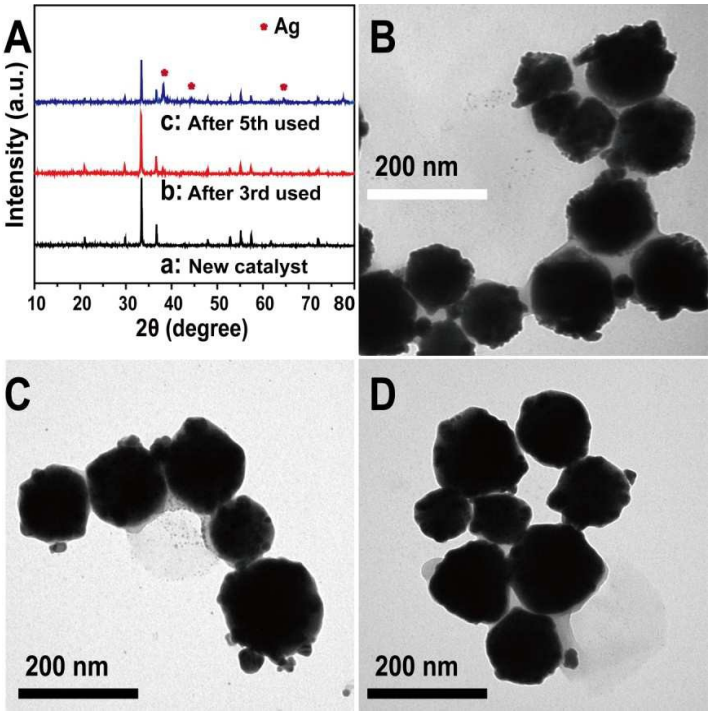

Fig. 7 (A) XRD patterns, (B-D) TEM images of the fresh Ag_3PO_4@BSG-30 nanocomposites, Ag_3PO_4@BSG-30 nanocomposites after third and fifth recycle experiments.

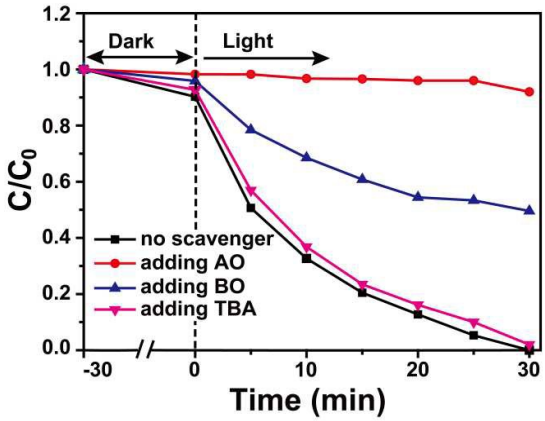

Fig. 8 Photocatalytic degradation curves of RhB over Ag_3PO_4@BSG-30 nanocomposites with different quenchers under visible light irradiation.

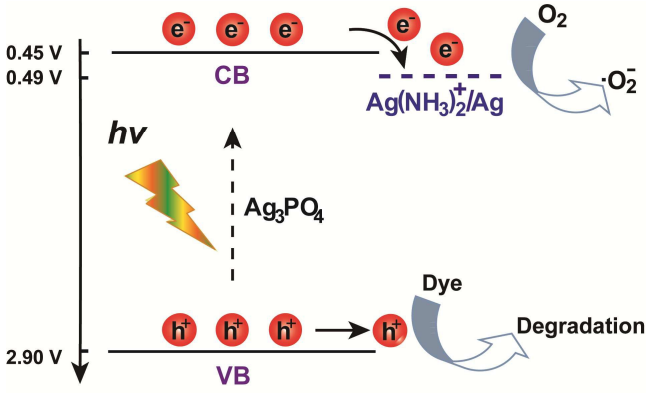

Fig. 9 Photocatalytic mechanism scheme of the Ag_3PO_4@BSG nanocomposites.

Graphical Abstract

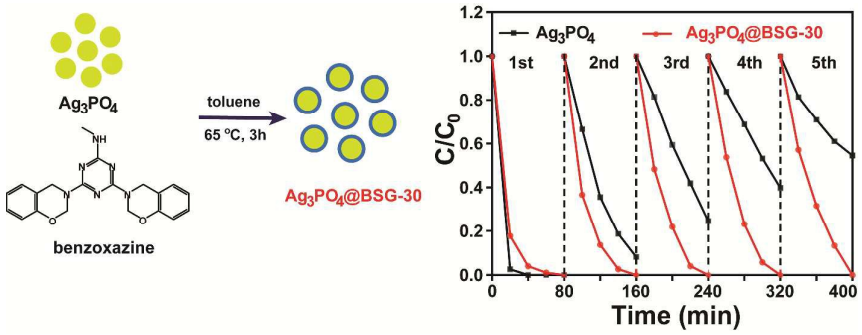

The Ag_3PO_4@BSG-30 nanocomposites exhibit a higher visible-light photocatalytic stability than the bare Ag_3PO_4 nanoparticles.